Cation effect on the inorganic–organic layered structure of pyrazole-4-sulfonate networks and inhibitory effects on copper corrosion†

Isurika R. Fernando,[a] Nikos Daskalakis,[b] Konstantinos D. Demadis*[b] and Gellert Mezei*[a]

Received (in Victoria, Australia) 23rd July 2009, Accepted 5th November 2009
First published as an Advance Article on the web 12th January 2010
DOI: 10.1039/b9nj00361d

The present study demonstrates that the pyrazole-4-sulfonate anion (4-SO_3-pzH = L^-) is a versatile ligand for the preparation of layered, 3-D solid state lattices. The ligand itself can coordinate to metals with both its sulfonate group and aromatic N-atom, as well as participate in hydrogen bonding both as donor and acceptor, and form various extended π–π networks. Five new complexes with Rb^+, Cs^+, Mg^{2+}, Sr^{2+} and Cu^{2+} have been prepared and characterized including single crystal X-ray diffraction: RbL, tetragonal $I4_1/a$, a = 9.7332(4) Å, b = 9.7332(4) Å, c = 29.941(1) Å, V = 2836.5(2) Å, Z = 16; CsL, monoclinic $P2_1/c$, a = 8.821(1) Å, b = 8.109(1) Å, c = 9.889(2) Å, β = 91.560(3)°, V = 707.1(2) Å, Z = 4; $Mg(H_2O)_6L_2$, triclinic $P\bar{1}$, a = 7.0543(7) Å, b = 7.7307(8) Å, c = 8.6389(9) Å, α = 72.572(2)°, β = 74.370(2)°, γ = 76.045(2)°, V = 426.22(8) Å, Z = 1; SrL_2, triclinic $P\bar{1}$, a = 6.027(2) Å, b = 7.243(3) Å, c = 14.186(5) Å, α = 92.491(8)°, β = 101.383(7)°, γ = 97.471(7)°, V = 426.22(8) Å, Z = 2; $Cu(H_2O)_2L_2{\cdot}4H_2O$, monoclinic $P2_1/c$, a = 9.032(1) Å, b = 13.297(1) Å, c = 7.7103(9) Å, β = 109.747(2)°, V = 871.5(2) Å, Z = 2. The varying size and charge of the cations in these five complexes produce unique, alternating inorganic–organic layered materials. We find a correlation between the size and charge of cations and the coordination mode of the ligand as well as hydration of the metal, but no correlation between the nature of the cation and the thickness of the inorganic/organic layers. We conclude that the overall 3-D structure of these layered materials is determined by a subtle balance between the coordination preferences of the metal ion and an intricate lattice of hydrogen bonds and aromatic interactions. Ligand HL and its complexes with Na, K, Rb, Cs, Mg, Ca, Sr and Ba were tested as potential corrosion inhibitors of copper metal surfaces at three different pH values (2, 3, and 4). All the above mentioned compounds show significant corrosion inhibition at pH 4 and 3, while no activity is observed at pH 2. The correlation of inhibition activity with pH of ligand HL and its different metal complexes is discussed.

Introduction

Continuous developments in supramolecular chemistry have led to the recognition of a variety of weak inter- or intra-molecular forces. Various types of hydrogen bonding,[1] halogen bonding,[2] aromatic-,[3] metal–metal (*e.g.*, aurophilic, argentophilic, *etc.*)[4] and other non-covalent interactions[5] are now sufficiently well understood and have become useful tools of the crystal engineer. However, the manipulation of several different kinds of such interactions at the same time, in order to create new materials with pre-designed structures and properties, remains a challenge. Two examples, where this deficiency is mostly felt, are the prediction of crystal structures and the tertiary structure of biological molecules, such as proteins and nucleic acids. Although weak compared to the covalent bond, such interactions are strong enough (especially when many of them are present) to determine the 3-D packing of molecules in the crystal lattice and to influence molecular conformations and coordination geometries. Therefore, a systematic study of the interplay between weak interactions is needed before understanding and mimicking Nature's more complex structures and functions.

Recently, we have initiated the previously unexplored solid state study of coordination networks formed by the pyrazole-4-sulfonate anion (4-SO_3-pzH = L^-), and observed the effect of cation size- and charge-variation on the 3-D structure of the Na, K, Ca and Ba-salts.[6] The pyrazole-4-sulfonate ligand combines the coordination flexibility of the sulfonate group with the ability of the pyrazole moiety (which can also coordinate to metals) to participate in hydrogen bonding and aromatic interactions (Scheme 1). The cation-induced changes are accommodated within a structurally adaptable framework of weak interactions and result in a rich variety in both the aromatic interactions as well as the sulfonate coordination modes within the distinct layered inorganic–organic

[a] *Department of Chemistry, Western Michigan University, Kalamazoo, Michigan 49008-5413, USA. E-mail: demadis@chemistry.uoc.gr*
[b] *Crystal Engineering, Growth & Design Laboratory, Department of Chemistry, University of Crete, Voutes Campus, Heraklion, Crete GR-71003, Greece. E-mail: gellert.mezei@wmich.edu*

† CCDC reference numbers 742361–742365. For crystallographic data in CIF or other electronic format see DOI: 10.1039/b9nj00361d

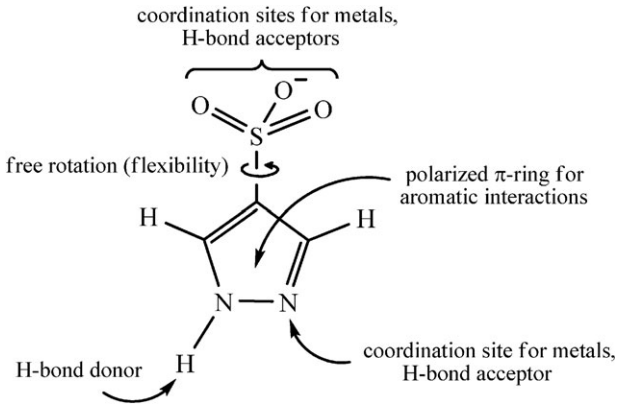

Scheme 1 Schematic illustration of the multiple binding modes of the pyrazole-4-sulfonate ligand L^-.

structure of these materials. Herein we report the synthesis and characterization of the alkali–metal Rb and Cs salts, alkaline-earth metal Mg and Sr salts as well as the transition-metal Cu(II) salt. We also report results of a systematic study on the inhibitory effect of these metal-pyrazole-4-sulfonates, as well as the Na, K, Ca, Ba analogs and the ligand HL itself, on the corrosion of copper metal. Copper corrosion is an industrially and economically significant process that can cause operational problems if left uncontrolled. Various anti-corrosion agents have been reported in the literature, with emphasis on heterocyclic aromatic compounds.[7] Ligand HL has been previously tested on iron surfaces at pH 0 and found to have anti-corrosion properties.[8]

Experimental

Materials and methods

All commercially available reagents were used as received. Pyrazole-4-sulfonic acid (HL) was prepared as described previously.[6,9] Elemental analyses were performed by Galbraith Laboratories, Inc., Knoxville, TN. Infrared, NMR and TGA spectra were recorded on a Bruker Equinox 55 FTIR (in KBr pellets), Jeol JNM-ECP400 (room temperature) and a Thermal Analyzer TGA Q500 instrument (heated at 10 °C min^{-1} from 25 to 700 °C under N_2), respectively. SEM/EDS studies were conducted on a scanning electron microscope LEO VP-35 FEM. pH was measured with a Mettler Toledo Seven Easy pH-meter (±0.01). pK_a was determined by pH titration. X-Ray diffraction data, collected at room temperature (298–301 K) from a single crystal mounted atop a glass fiber with either a Siemens SMART 1 K CCD or a Bruker SMART APEX II diffractometer using graphite-monochromated Mo-Kα (λ = 0.71073 Å) radiation were corrected for Lorentz and polarization effects. The structures were solved employing the SHELXTL-direct methods program and refined by full-matrix least-squares on F^2.[10] Crystallographic details are summarized in Table 1.

Synthesis and characterization

Dissolution of HL and the corresponding alkali, alkaline-earth or copper compounds (Rb_2CO_3, $CsOH{\cdot}H_2O$, MgO, $SrCO_3$ and $CuCO_3{\cdot}Cu(OH)_2$, respectively) in the required molar ratios in H_2O provides the Rb, Cs, Mg, Sr and Cu salts in quantitative yield after removal of the solvent. Colorless or blue (copper complex) crystals suitable for X-ray diffraction study are obtained either by slow evaporation of aqueous solutions ($Mg(H_2O)_6L_2$, SrL_2 and $CuL_2(H_2O)_2{\cdot}4H_2O$), crystallization from H_2O–EtOH (1 : 1) (RbL) or evaporation of an aqueous solution at ~90 °C in an oven (CsL).

$Mg(H_2O)_6L_2$. For $C_6H_{18}MgN_4O_{12}S_2$, calculated/found: C, 16.89/16.81%; H, 4.26/4.35%; N, 13.15/13.24%. IR (KBr, cm^{-1}): 3432 s (br), 3124 s (br), 2882 s, 1662 s, 1544 m, 1473 m, 1395 m, 1237 s, 1196 s, 1089 s, 1054 s, 1060 s, 958 m, 904 m, 865 m, 797 m, 743 m, 660 s, 555 m. ^{1}H-NMR (400 MHz, D_2O): 7.93 ppm (s, 2H). **SrL_2**: For $C_6H_6N_4O_6S_2Sr$, calculated/found: C, 18.87/18.66%; H, 1.58/1.71%; N, 14.68/14.49%. IR (KBr, cm^{-1}): 3141 s, 3071 s, 2997 s, 2938 s, 2881 s, 2831 s, 1650 m, 1554 m, 1492 m, 1391 m, 1221 s, 1182 s, 1071 s, 964 m, 896 m, 837 m, 665 s, 558 m. ^{1}H-NMR (400 MHz, D_2O): 7.93 ppm (s, 2H). **RbL**: For $C_3H_3N_2O_3RbS$, calculated/found: C, 15.49/15.28%; H, 1.30/1.39%; N, 12.05/11.98%. IR (KBr, cm^{-1}): 3356 s (br), 3160 m, 1728 w, 1533 m, 1459 m,

Table 1 Summary of crystallographic data for metal–L compounds

	$Mg(H_2O)_6L_2$	SrL_2	RbL	CsL	$Cu(H_2O)_2L_2{\cdot}4H_2O$
Formula	$C_6H_{18}MgN_4O_{12}S_2$	$C_6H_6N_4O_6S_2Sr$	$C_3H_3N_2O_3RbS$	$C_3H_3CsN_2O_3S$	$C_6H_{18}CuN_4O_{12}S_2$
Formula weight	426.67	381.89	232.60	280.04	465.90
Crystal system	Triclinic	Triclinic	Tetragonal	Monoclinic	Monoclinic
Space group	$P\bar{1}$ (No. 2)	$P\bar{1}$ (No. 2)	$I4_1/a$ (No. 88)	$P2_1/c$ (No. 14)	$P2_1/c$ (No. 14)
a/Å	7.0543(7)	6.027(2)	9.7332(4)	8.821(1)	9.032(1)
b/Å	7.7307(8)	7.243(3)	9.7332(4)	8.109(1)	13.297(1)
c/Å	8.6389(9)	14.186(5)	29.941(1)	9.889(2)	7.7103(9)
α/°	72.572(2)	92.491(8)	90	90	90
β/°	74.370(2)	101.383(7)	90	91.560(3)	109.747(2)
γ/°	76.045(2)	97.471(7)	90	90	90
V/Å^3	426.22(8)	600.4(4)	2836.5(2)	707.1(2)	871.5(2)
Z	1	2	16	4	2
D_c/g cm^{-3}	1.662	2.112	2.179	2.631	1.775
μ/mm^{-1}	0.417	4.867	7.223	5.479	1.559
Reflections collected/unique	2057/1225	2757/1719	62 644/1942	3733/1247	3709/1252
Observed reflections ($I > 2\sigma(I)$)	1101	1622	1643	1140	1180
Goodness-of-fit (on F^2)	1.063	1.081	0.970	1.085	1.062
$R(F)$; $R_w(F)$ ($I > 2\sigma(I)$)	0.0326; 0.0886	0.0253; 0.0660	0.0257; 0.1175	0.0191; 0.0479	0.0238; 0.0658

1386 m, 1218 s, 1115 s, 1062 s, 930 m, 869 m, 766 m, 661 s, 551 m. ^{1}H-NMR (400 MHz, D_2O): 7.93 ppm (s, 2H). **CsL**: For $C_3H_3CsN_2O_3S$, calculated/found: C, 12.86/13.12%; H, 1.08/1.20%; N, 10.01/10.56%. IR (KBr, cm^{-1}): 3210 s, 3138 m, 3071 m, 3005 m, 2961 m, 2876 m, 2828 m, 1549 m, 1491 m, 1381 m, 1230 s, 1180 s, 1052 s, 964 m, 936 m, 862 m, 779 m, 654 s, 548 m. ^{1}H-NMR (400 MHz, D_2O): 7.93 ppm (s, 2H). **$CuL_2(H_2O)_2{\cdot}4H_2O$**: For $C_6H_{18}CuN_4O_{12}S_2$, calculated/found: C, 15.46/15.27%; H, 3.90/3.98%; N, 12.03/11.89%. IR (KBr, cm^{-1}): 3237 s, 3131 m, 3004 w, 2928 w, 1726 w, 1646 w, 1539 m, 1473 m, 1403 m, 1276 m, 1239 s, 1195 s, 1133 s, 1076 s, 1043 m, 970 m, 863 m, 799 w, 670 s, 605 s, 570 m, 537 m.

Corrosion inhibition protocols

A modified protocol based on the National Association of Corrosion Engineers (NACE) Standard TM0169-95 is used.[11] Corrosion specimens (copper metal, grade 99.999%, 1 mm thin foil) are cut into 2 × 2 cm squares and prepared according to the well-established protocol mentioned above. Each specimen is immersed in a control aqueous solution (no inhibitor) or in a test solution (0.50 mM in L or metal–L complex) at pH = 2, 3 or 4, respectively, and corrosion progress is monitored by visual inspection for a number of days. The duration of the corrosion experiments is variable. For example, for the experiments at pH 2, duration was ~4 days, at pH 3 it was 14–18 days (depending on individual experiments), and at pH 4 it was 18–19 days (depending on individual experiments). Longer experiment times were required for the pH 3 and 4 experiments since copper corrosion becomes slower at higher pH values. Then, the specimens were removed from solution, surface samples were taken for spectroscopic studies and the corrosion products were cleaned off the copper surface by the standard NACE method referenced above in order to determine corrosion rates from mass loss. The experimental error for this technique is ±5%. The corrosion experiments were repeated and the copper specimens were used for optical microscopy, scanning electron microscopy (SEM) and energy dispersive X-ray spectroscopy (EDS) studies.

Results

Reaction of pyrazole-4-sulfonic acid in aqueous solution with Rb_2CO_3, $CsOH{\cdot}H_2O$, MgO, $SrCO_3$ and $CuCO_3{\cdot}Cu(OH)_2$, respectively, provides the corresponding metal–sulfonate complexes, obtained as colorless or blue ($CuL_2(H_2O)_2{\cdot}4H_2O$) crystals after water evaporation. All complexes are soluble in water, dimethylsulfoxide and ethylene glycol, but insoluble in other common organic solvents, with the exception of the Mg salt which also dissolves in the polar solvents methanol, ethanol and dimethylformamide. The anhydrous complexes are thermally stable up to 230–290 °C without melting.

Structure description

Rb(4-SO_3-pzH). There are two independent Rb atoms in the structure of RbL, both lying on two-fold axes. Each Rb ion is eight-coordinate by six O-atoms from four different SO_3^- groups and two N-atoms from two pyrazole moieties (Fig. 1 and 2, Table 2). The structure of the inorganic layer (Fig. 3) is built on an undulating, approximately rectangular

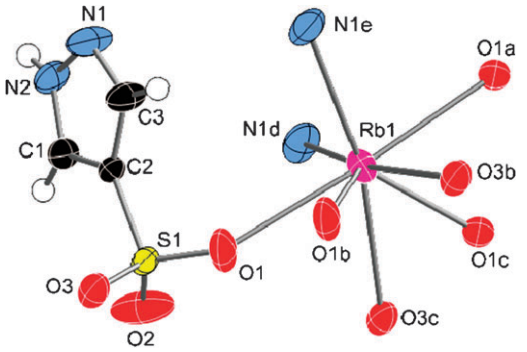

Fig. 1 Thermal ellipsoid plot (50% probability) of RbL, showing the coordination sphere around Rb1 (which is the same as the one around Rb2, with slightly different bond lengths). Symmetry codes: (a) $-x + 1$, $-y + 1.5$, z; (b) $-x + 1$, $-y + 2$, $-z$; (c) x, $y - 0.5$, $-z$; (d) $y - 0.25$, $-x + 1.25$, $-z + 0.25$; (e) $-y + 1.25$, $x + 0.25$, $-z + 0.25$.

array of Rb ions (within each rectangle, Rb–Rb distances: 4.993(1), 4.867(1), 5.018(1) and 4.867(1) Å; Rb–Rb–Rb angles: 90.14(1) and 89.85(1)°). The Rb rectangles are bridged on alternating sides by μ_4-sulfonate and μ_2-pyrazole groups. The rather long Rb–N bonds (3.213(3) and 3.290(3) Å) are not uncommon, as even Rb–N bonds longer than 3.4 Å have been reported.[12] The bifurcated binding mode of the heterocyclic N-atom has also been documented.[13] Within the organic layer, the pyrazole moieties are organized in a T-stacked pattern by edge-to-face aromatic interactions (Fig. 4), with the closest contacts of H1···N2: 2.85 Å and H3···C2: 2.97 Å (H–centroid distances are 2.80 and 3.27 Å, respectively). The N–H hydrogen atom forms a bifurcated hydrogen bond to two sulfonate O-atoms (Table 3).

Cs(4-SO_3-pzH). The Cs ion is nine-coordinate by seven O-atoms from five different SO_3^- groups and two N-atoms from two pyrazole moieties (Fig. 5 and 2, Table 4). The inorganic layer (Fig. 3) consists of a zigzagging pattern of Cs ions at distances of 4.564(1), 4.829(1) and 5.117(1) Å from each other, bridged on both sides by μ_5-sulfonate and μ_2-pyrazole groups. The rather long Cs–N bonds (3.412(3) and 3.503(3) Å) are not uncommon, as even Cs–N bonds longer than 3.6 Å have been observed.[14] Similarly to the case of the Rb analog, several examples of the bifurcated binding mode of the heterocyclic N-atom to cesium are known.[13a-c,15] Within the organic layer, the pyrazole moieties are organized in a sandwich-herringbone pattern by edge-to-face aromatic interactions (Fig. 4), with the closest contacts of H1···N2: 2.85 Å and H3···C2: 2.97 Å (H–centroid distances are 2.80 and 3.27 Å, respectively). The N–H hydrogen atom forms a hydrogen bond to a sulfonate oxygen atom (Table 3).

$Mg(H_2O)_6$(4-SO_3-pzH)$_2$. The Mg ion, which lies on an inversion center, is six-coordinate by water molecules and it does not bind directly to sulfonate groups (Fig. 6 and 2, Table 5). The inorganic layer (Fig. 3) is comprised of a planar array of $[Mg(H_2O)_6]^{2+}$ units (shortest Mg–Mg distance: 7.731(1) Å) interconnected by sulfonate groups on either side. All three oxygen atoms of the sulfonate groups participate in hydrogen bonding to a total of four coordinated H_2O molecules; the hydrogen bonding distances range from 1.98(1) to

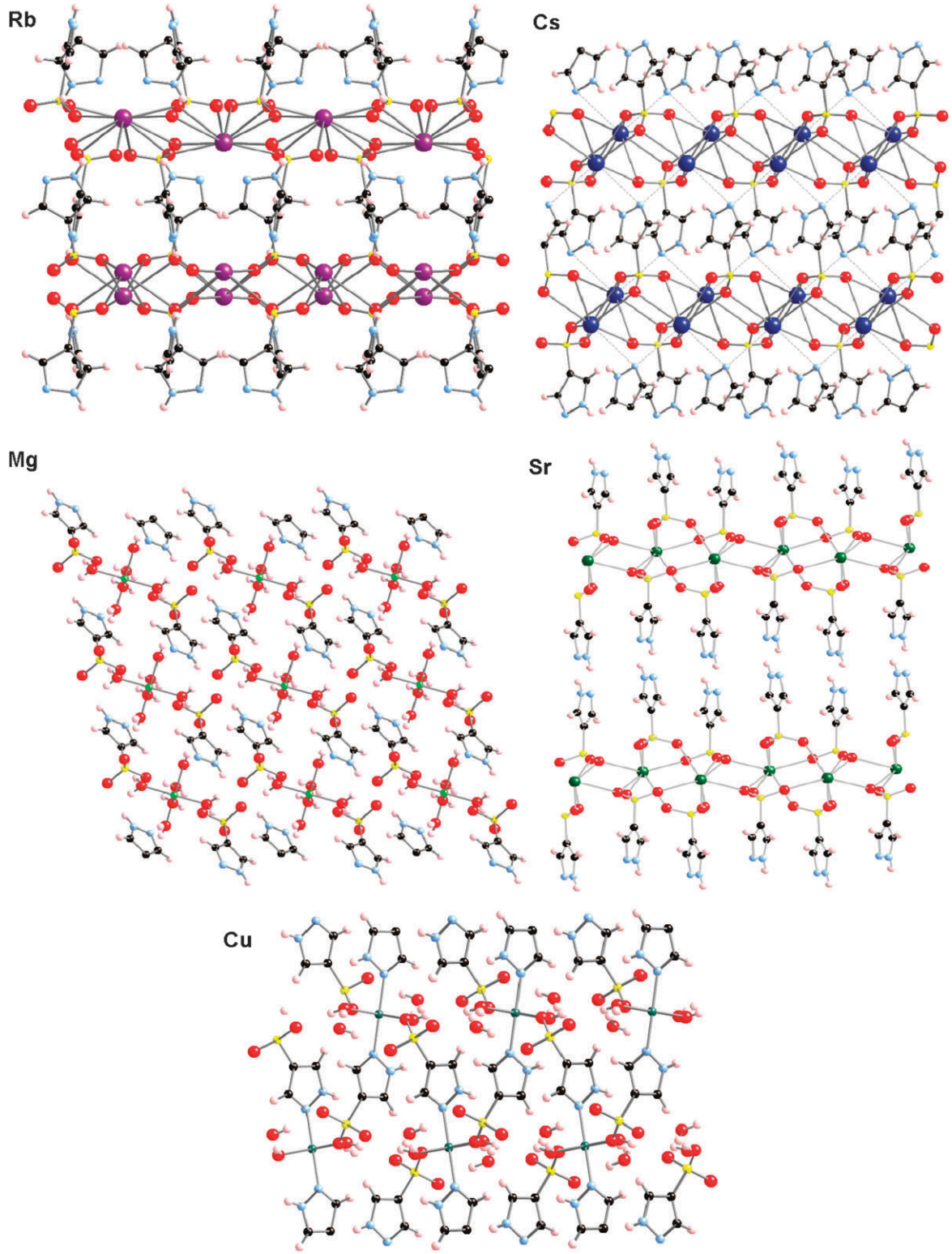

Fig. 2 Side view of the alternating inorganic–organic layered structures of RbL, CsL, $Mg(H_2O)_6L_2$, SrL_2 and $CuL_2(H_2O)_2{\cdot}4H_2O$.

2.12(1) Å (with O···O distances of 2.78(1) to 2.90(1) Å). The remaining two coordinated H_2O molecules form hydrogen bonds with the pyrazole N-atom. Within the organic layer (Fig. 4), the pyrazole moieties form pairs of parallel π–π stacks, with very weak inter-pair interactions (closest contact is H3···C3: 3.56 Å, H–centroid distance: 4.05 Å). The N–H hydrogen atoms of the pyrazole moieties form hydrogen bonds to the sulfonate groups (Table 3).

$Sr(4\text{-}SO_3\text{-}pzH)_2$. The Sr ion is eight-coordinate by seven different SO_3^- groups (Fig. 7 and 2, Table 6). The inorganic layer (Fig. 3) contains Sr ions arranged in a zigzag pattern

Table 2 Selected bond lengths (Å) for RbL

Rb1–O1	2.796(2)	Rb2–O2	2.908(3)	S1–O1	1.438(3)
Rb1–O3b	2.996(2)	Rb2–O2f	3.007(3)	S1–O2	1.438(2)
Rb1–O1b	3.202(3)	Rb2–O3c	3.083(2)	S1–O3	1.442(2)
Rb1–N1d	3.213(3)	Rb2–N1d	3.290(3)		

Symmetry transformations used to generate equivalent atoms: (a) $-x + 1, -y + 1.5, z$; (b) $-x + 1, -y + 2, -z$; (c) $x, y - 0.5, -z$; (d) $y - 0.25, -x + 1.25, -z + 0.25$; (e) $-y + 1.25, x + 0.25, -z + 0.25$; (f) $-x, -y + 1, -z$.

(shortest Sr–Sr distance: 4.273(1) Å) bridged on either side by μ_3- and μ_4-sulfonate groups. The organic layer is comprised of a double-layer of pyrazole groups, a unique feature among the pyrazole–sulfonate structures studied so far (Fig. 2). Within each half of the organic layer, the pyrazole moieties are organized in a herringbone pattern by edge-to-face aromatic interactions (Fig. 4), with the closest contacts of H1···N3: 2.92 Å, H3···N4: 3.03 Å and H4a···C2: 2.95 Å (H–centroid distances are 3.05, 2.91 and 3.35 Å, respectively). The two halves of the organic layer are interconnected by hydrogen bonds between zigzag strands of pyrazole groups (Fig. 8, Table 3).

$Cu(4\text{-}SO_3\text{-}pzH)_2(H_2O)_2{\cdot}4H_2O$. The Cu(II) ion, which lies on an inversion center, is six-coordinate by four O-atoms (two from sulfonate groups and two from water molecules) and two pyrazole N-atoms. The coordination geometry around the metal is axially elongated octahedral, with the sulfonate groups in axial positions (Fig. 9 and 2, Table 7). Within the inorganic layer, the Cu ions are arranged in a linear pattern (7.710(2) and 9.031(2) Å from each other) and are interconnected by an extended hydrogen-bonded network of sulfonate groups and water molecules (Fig. 3). Two O-atoms of each sulfonate group participate in four hydrogen bonds with three water molecules (Table 3). An even stronger hydrogen bond is formed between a coordinated and a lattice water molecule. Within the organic layer, pyrazole moieties form infinite π-stacked columns (with centroid–centroid distances of 3.869 Å) (Fig. 4). These columns are separated from each other by water molecules hydrogen-bonded to the pyrazole N–H groups; the water molecules also form two weaker hydrogen bonds to a sulfonate group and another water molecule. This is the first pyrazole–sulfonate structure studied in which the organic layer, comprised of pyrazole moieties, incorporates water molecules.

Spectral and thermogravimetric analysis

The infrared spectra of the complexes show strong bands in the 1240–1180 cm^{-1} region corresponding to vibrations of the sulfonate group.[16] C–H stretching vibrations are observed in the 3160–2830 cm^{-1} region. Bands attributed to vibrations of the pyrazole rings spread over the regions 1670–1380 and 1130–530 cm^{-1}. The hydrated complexes show broad absorption bands around 3400 cm^{-1}, characteristic of the stretching vibrations of N–H and O–H groups involved in extensive hydrogen bonding. The absence of these bands in the spectrum of the Rb, Cs and Sr complexes confirms their anhydrous solid state lattice determined by X-ray diffraction.

^{1}H-NMR shows one singlet at 7.93 ppm for the Rb, Cs, Mg and Sr salts corresponding to the aromatic C–H proton. The invariance of the chemical shift with varying metal ions points to an ionic behavior of these complexes in aqueous solution.

Thermogravimetric analysis (TGA) shows sequential loss of the six water molecules for both $Mg(H_2O)_6L_2$ and $Cu(H_2O)_2L_2{\cdot}4H_2O$. In the case of the Mg salt, four H_2O molecules are lost from 65 to 130 °C, while the remaining two H_2O molecules are lost between 185 and 230 °C (calc. 25%, obs. 25%). In the case of the Cu salt, the loss of the four interstitial H_2O molecules starts at room temperature and is complete by 75 °C (calc. 15%, obs. 14%). The complete loss of these four water molecules is also observed upon prolonged standing at room temperature. The two coordinated H_2O molecules are lost between 175–200 °C (calc. 8%, obs. 8%). The anhydrous salts (MgL_2, SrL_2, RbL, CsL and CuL_2) are stable up to 270, 250, 230, 255 and 350 °C, respectively. Decomposition occurs above those temperatures, leaving behind the corresponding metal sulfates.

Copper corrosion inhibition efficiency

The corrosion inhibition efficiency of all materials described herein was quantified as the "corrosion rate" (CR), by using the equation:

$$CR = 87.6 \times \frac{(\text{mass loss})}{(\text{area})(\text{time})(\text{metal density})}$$

Units: CR in mm/year, mass loss in mg, area in cm^2, time in hours, metal density = 8.94 g cm^{-3} (for Cu).

Examination of CRs at pH 2 (Fig. 10) reveals that none of the metal–L materials inhibit corrosion at this pH, as all CRs are either the same as, or higher than the control (no inhibitor). RbL, CsL, MgL_2 and BaL_2 act as copper oxide dissolvers and not as corrosion inhibitors, as evidenced by the higher corrosion rates. As the pH is increased from 2 to 3, the corrosion rate for the control is lowered dramatically. This is expected as corrosion rates strongly depend on pH and are lower as the pH of the solution increases.[17] The metal–L additives demonstrate substantial corrosion inhibition with CRs in the range of 0.05–0.08 mm/year. This should be compared to the CR for the control (0.31 mm/year) and for HL (0.05 mm/year). There appears to be no dramatic differentiation in anti-corrosion efficiency among the metal–L additives. When a control corrosion experiment is performed at pH 4, CR is further reduced (to 0.11 mm/year), as expected. When HL is used as the additive, further reduction of CR (to 0.08 mm/year) is measured. Presence of metal–L additives causes yet further reduction in CRs that range from 0.01 to 0.08 mm/year.

Study of protective films

After removal from the corresponding solutions, the copper surfaces were photographed in each experiment. Images from the pH 4 experiments, shown in Fig. 11, demonstrate that all surfaces are satisfactorily protected in the presence of HL or metal–L complexes. The "control" surface has an obvious layer of green copper-patina. All other surfaces are clean from corrosion products. Slight discolorations can be noted, but these are not caused by ineffective corrosion protection.

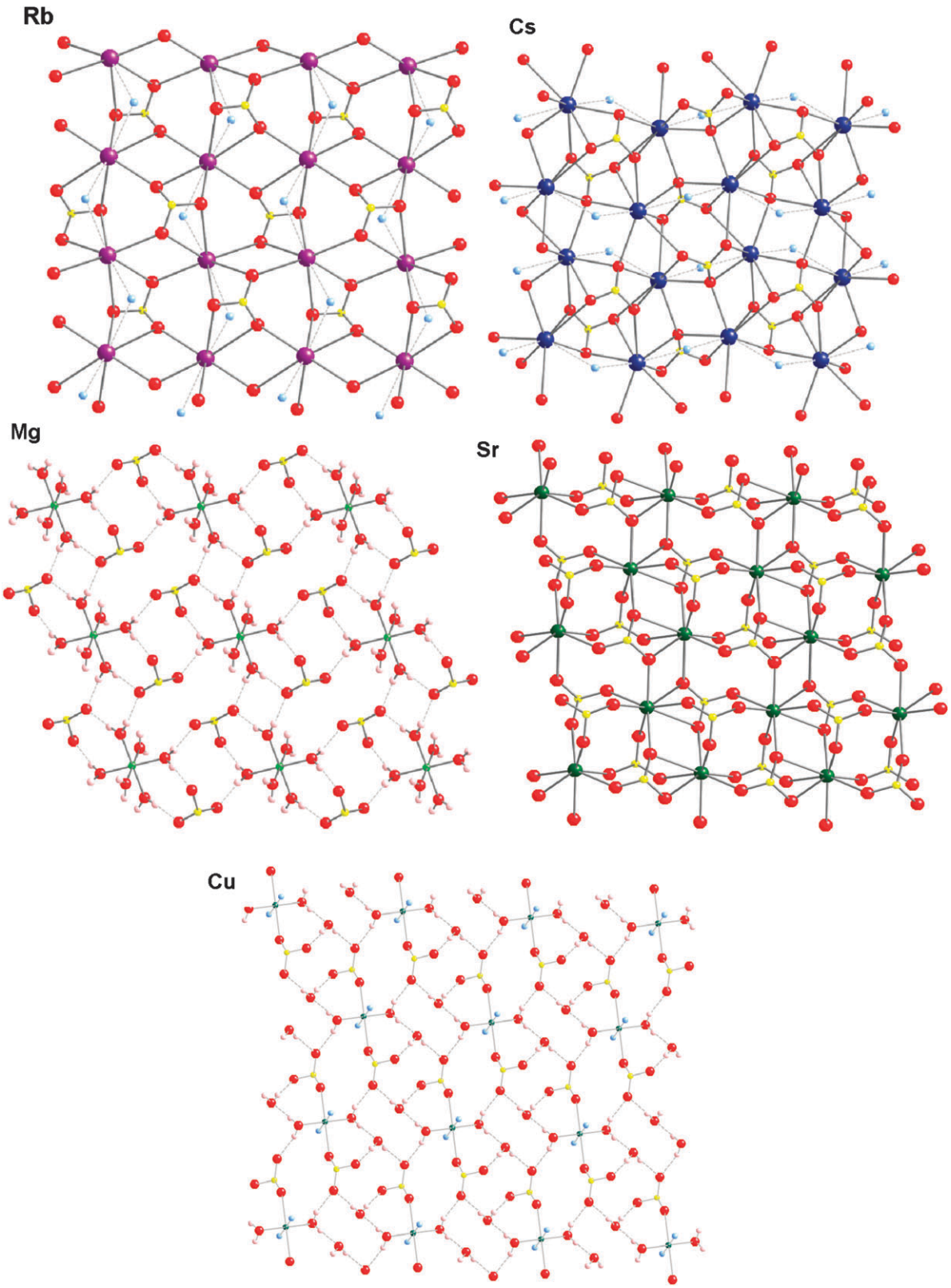

Fig. 3 Perpendicular view to the inorganic layer in RbL, CsL, $Mg(H_2O)_6L_2$, SrL_2 and $CuL_2(H_2O)_2{\cdot}4H_2O$.

Copper specimens were also subjected to SEM/EDS studies. EDS has been previously proven to be very useful in studying the composition of anti-corrosion coatings.[18] Representative SEM images of the protective films are shown in Fig. 12. The control copper specimen had a rough film of copper oxide (identified by EDS), which was visible by both optical microphotography and SEM (see image "control"). In the presence of either HL alone (see image "HL") or

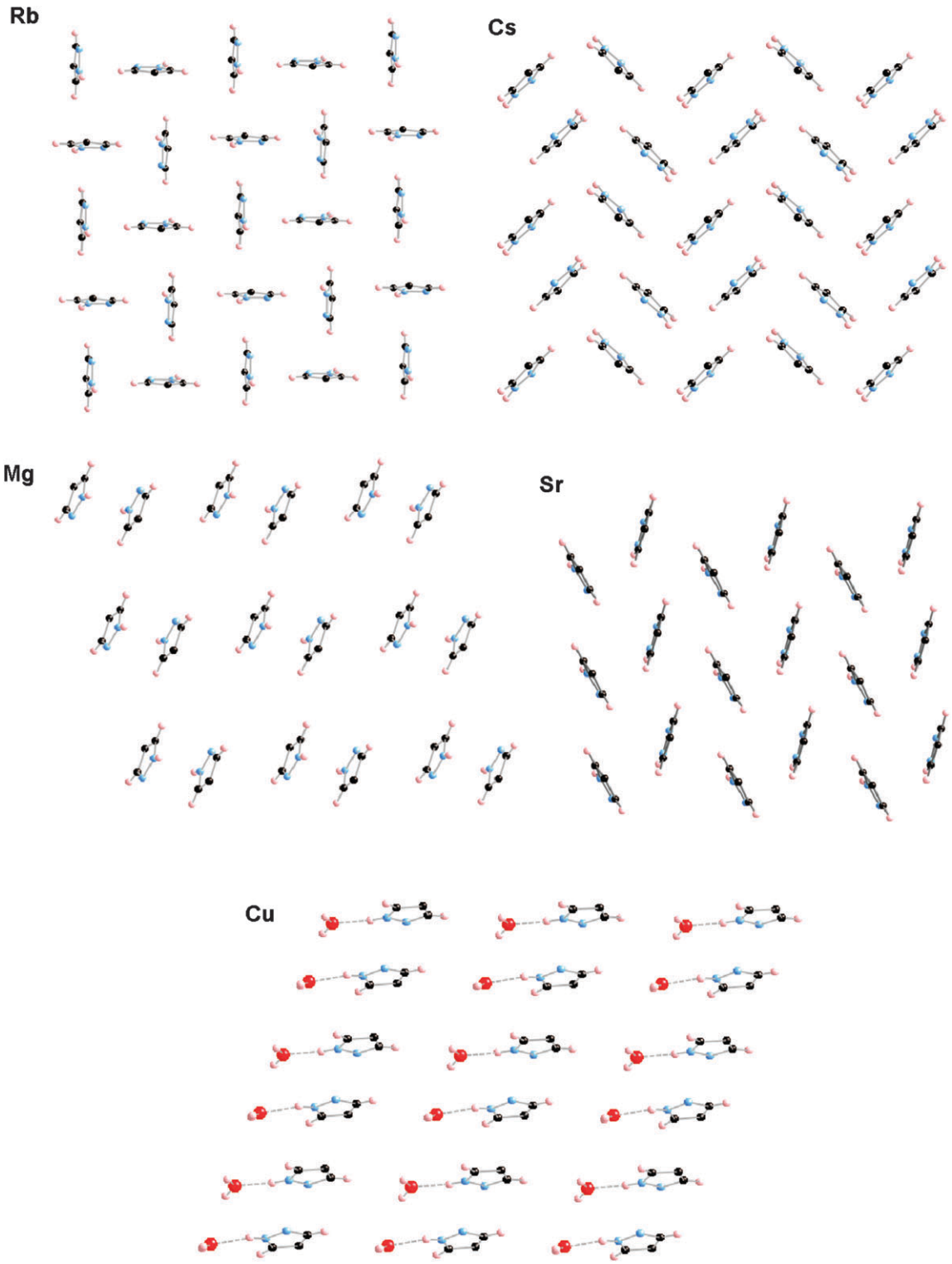

Fig. 4 Perpendicular view to the organic layer in RbL, CsL, $Mg(H_2O)_6L_2$, SrL_2 and $CuL_2(H_2O)_2{\cdot}4H_2O$, illustrating the various aromatic interaction patterns.

metal–L, the surface morphology reveals a much smoother film composed of ~100 nm sized particles (for HL and KL) or larger particles (~200 nm for RbL and > 400 nm for CsL). The SrL_2 protective film appears very compact with continuous surface coverage with only some areas showing presence of pores (right side of image "SrL_2"). EDS revealed the presence of the respective cation used in each experiment, thus confirming the formation of metal–L protective films. The protective films have also been studied by FT-IR spectroscopy and the spectra were compared to those of the authentic metal–L materials. Comparative results for the SrL_2-film and an authentic sample of SrL_2 are shown in

Table 3 Summary of hydrogen bonding data for metal–L compounds

Compound	D–H···A	D–H/Å	H···A/Å	D···A/Å	D–H···A/°	Sym. oper. for A
RbL	N2 H2 O1	0.86	2.36	3.082(4)	142	$3/4 - y, 1/4 + x, 1/4 + z$
	N2 H2 O3	0.86	2.36	2.922(3)	126	$1/4 - y, 1/4 + x, 1/4 - z$
CsL	N2 H2 O1	0.86	2.01	2.799(4)	152	$1 - x, -1/2 + y, 3/2 - z$
$Mg(H_2O)_6L_2$	N2 H2 O2	0.86	2.31	3.110(3)	156	$-1 + x, y, z$
	O4 H4A O3	0.82	2.02	2.834(3)	172	$1 - x, 1 - y, 1 - z$
	O4 H4B O3	0.80	2.00	2.798(2)	170	
	O5 H5A O1	0.82	1.99	2.811(3)	174	$x, -1 + y, z$
	O5 H5B O2	0.82	1.98	2.785(2)	167	$1 - x, 1 - y, -z$
	O6 H6A N1	0.81	1.97	2.776(3)	174	$-x, -y, 1 - z$
	O6 H6B O1	0.80	2.12	2.902(3)	164	$-x, 1 - y, 1 - z$
SrL_2	N2 H2 N3	0.86	2.12	2.950(4)	163	x, y, z
	N4 H4 N1	0.86	2.06	2.899(4)	166	$-1 + x, y, 1 + z$
$Cu(H_2O)_2L_2{\cdot}4H_2O$	O4 H4A O1	0.79	1.94	2.699(2)	160	$x, 1/2 - y, 1/2 + z$
	O4 H4B O5	0.80	1.85	2.644(2)	175	$x, y, -1 + z$
	O5 H5A O1	0.83	1.96	2.777(3)	170	$-x, 1/2 + y, 1/2 - z$
	O5 H5B O3	0.79	1.93	2.725(2)	174	$x, 1/2 - y, 1/2 + z$
	O6 H6A O5	0.80	2.13	2.920(3)	173	$1 + x, y, z$
	O6 H6B O3	0.80	2.20	2.954(3)	156	$1 + x, y, 1 + z$
	N2 H2 O6	0.86	2.00	2.808(3)	157	$x, y, -1 + z$

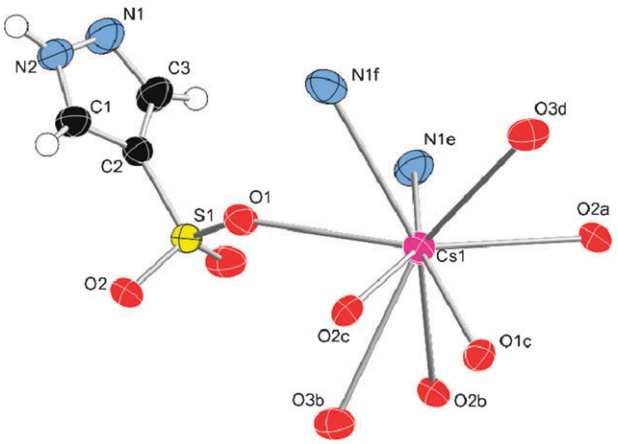

Fig. 5 Thermal ellipsoid plot (50%) of CsL, showing the coordination sphere around cesium. Symmetry codes: (a) $x, y + 1, z$; (b) $-x, -y + 1, -z + 1$; (c) $-x, y + 0.5, -z + 1.5$; (d) $x, -y + 1.5, z + 0.5$; (e) $-x + 1, -y + 1, -z + 1$; (f) $-x + 1, y + 0.5, -z + 1.5$.

Table 4 Selected bond lengths (Å) for CsL

Cs1–O1	3.204(2)	Cs1–O2c	3.176(2)	Cs1–N1f	3.503(3)
Cs1–O1c	3.225(2)	Cs1–O3b	3.361(3)	S1–O1	1.462(2)
Cs1–O2a	3.130(2)	Cs1–O3d	3.370(2)	S1–O2	1.453(2)
Cs1–O2b	3.132(2)	Cs1–N1e	3.412(3)	S1–O3	1.446(2)

Symmetry transformations used to generate equivalent atoms: (a) $x, y + 1, z$; (b) $-x, -y + 1, -z + 1$; (c) $-x, y + 0.5, -z + 1.5$; (d) $x, -y + 1.5, z + 0.5$; (e) $-x + 1, -y + 1, -z + 1$; (f) $-x + 1, y + 0.5, -z + 1.5$.

Fig. 13. Similar results were obtained for the other metal–L films and compounds as well. There is a good agreement between the two spectra, as indicated by the dashed lines. Small shifts of a number of peaks, as well as different intensities may be due to the fact that the strontium–L film was formed under different conditions than bulk SrL_2, resulting in changes in hydrogen bonding and relative extent of film hydration.

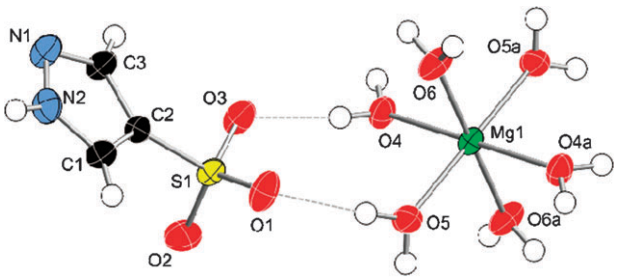

Fig. 6 Thermal ellipsoid plot (50%) of $Mg(H_2O)_6L_2$, showing the coordination sphere around magnesium. Symmetry codes: (a) $-x, -y + 2, -z + 1$.

Table 5 Selected bond lengths (Å) for $Mg(H_2O)_6L_2$

Mg1–O4	2.066(2)	S1–O1	1.452(2)
Mg1–O5	2.066(2)	S1–O2	1.447(2)
Mg1–O6	2.047(2)	S1–O3	1.454(2)

Symmetry transformation used to generate equivalent atoms: (a) $-x, -y + 2, -z + 1$.

Discussion

Structure of the inorganic layer and comparison with related metal–sulfonate complexes

All pyrazole-4-sulfonate metal complexes studied so far show a layered inorganic–organic structure. Within the inorganic layer, the metal ions are coordinated by sulfonate groups and/or water molecules and in some cases by pyrazole groups. As illustrated in Table 8, the coordination number around the metal ions increases with both the ionic radius and charge.[19] Within the alkali metal complex series studied here, the smallest Na^+ ion is 6-coordinate while the largest Cs^+ ion is 9-coordinate. In the case of the alkaline-earth metal complex series studied here, the smallest Mg^{2+} ion is 6-coordinate and the largest Ba^{2+} ion is 10-coordinate. For ions with similar

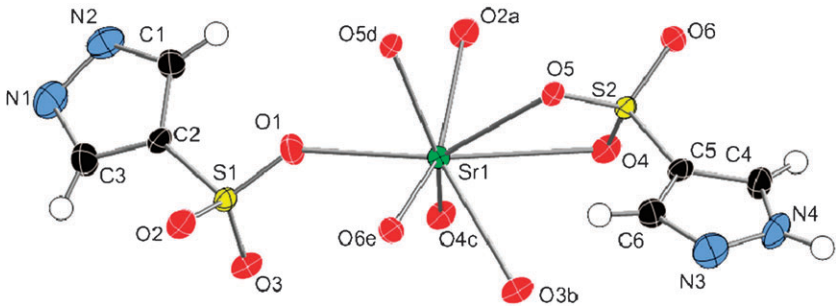

Fig. 7 Thermal ellipsoid plot (50%) of SrL_2, showing the coordination sphere around strontium. Symmetry codes: (a) $x - 1, y, z$; (b) $-x + 1, -y + 2, -z + 1$; (c) $-x, -y + 2, -z + 1$; (d) $-x, -y + 1, -z + 1$; (e) $x + 1, y, z$.

Table 6 Selected bond lengths (Å) for SrL_2

Sr1–O1	2.528(2)	Sr1–O5	2.599(2)	S1–O3	1.454(3)
Sr1–O2a	2.526(2)	Sr1–O5d	2.587(2)	S1–O4	1.463(2)
Sr1–O3b	2.643(2)	Sr1–O6e	2.512(2)	S1–O5	1.467(2)
Sr1–O4	2.921(2)	S1–O1	1.451(2)	S1–O6	1.440(2)
Sr1–O4c	2.550(2)	S1–O2	1.451(2)		

Symmetry transformations used to generate equivalent atoms: (a) $x - 1, y, z$; (b) $-x + 1, -y + 2, -z + 1$; (c) $-x, -y + 2, -z + 1$; (d) $-x, -y + 1, -z + 1$; (e) $x + 1, y, z$.

radii (Na^+/Ca^{2+} and K^+/Ba^{2+}), the coordination number of the doubly charged ion is one or two units higher than the coordination number of the singly charged ion, respectively. The number of coordinated water molecules decreases with increasing cation size, from six for the smaller Mg^{2+} ion to zero for the larger Rb^+, Cs^+ and Sr^{2+} ions. The hapticity of the sulfonate ligand is directly proportional to cation size and inversely proportional to the number of coordinated water molecules. No sulfonate coordination is observed for the small Mg^{2+} ion surrounded by six water molecules, and only terminal coordination is seen for the similarly sized Cu^{2+} ion coordinated by two H_2O molecules. With increasingly larger ions, the sulfonate groups adopt μ_2-, μ_3-, μ_4- and even μ_5-bridging coordination modes and for the ones larger than 1.51 Å, a chelating mode is also observed. The hapticity increases up to μ_5-η^3:η^2:η^2 in case of the largest and anhydrous Cs^+ ion (Scheme 2).

A similar correlation of the size and charge of the metal ion with the number of coordinated water molecules and hapticity of the sulfonate group is found in the case of other metal–sulfonate complexes. For example, in the series of *p*-toluenesulfonates (tosylates), small divalent cations are 6-coordinate

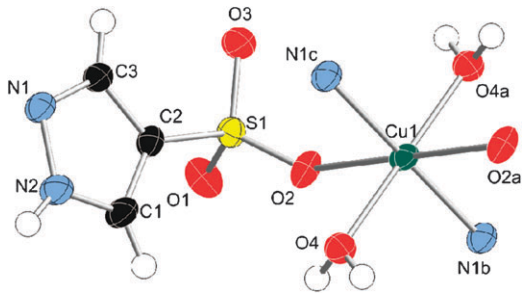

Fig. 9 Thermal ellipsoid plot (50%) of $CuL_2(H_2O)_2{\cdot}4H_2O$, showing the coordination sphere around copper. Symmetry codes: (a) $-x + 1, -y + 1, -z + 2$; (b) $-x + 1, y - 0.5, -z + 2.5$; (c) $x, -y + 1.5, z - 0.5$.

Table 7 Selected bond lengths (Å) for $Cu(H_2O)_2L_2{\cdot}4H_2O$

Cu1–O2	2.412(2)	S1–O1	1.456(2)
Cu1–O4	1.968(2)	S1–O2	1.450(2)
Cu1–N1b	2.009(2)	S1–O3	1.450(2)

Symmetry transformations used to generate equivalent atoms: (a) $-x + 1, -y + 1, -z + 2$; (b) $-x + 1, y - 0.5, -z + 2.5$; (c) $x, -y + 1.5, z - 0.5$.

and form isostructural complexes containing $[M(H_2O)_6]^{2+}$ species with no direct sulfonate coordination (ionic radii are given in parentheses): Mg^{2+} (0.72 Å), Mn^{2+} (0.83 Å), Fe^{2+} (0.78 Å), Co^{2+} (0.74 Å), Ni^{2+} (0.69 Å), Cu^{2+} (0.73 Å), Zn^{2+} (0.74 Å).[20,21] Sc^{3+} has a similar ionic radius (0.72 Å) and is also 6-coordinate, but it has two η^1-sulfonate groups and four H_2O molecules coordinating.[22] This could be attributed to the higher charge (3+) compared to the previous metals (2+). Very small trivalent cations such as Ti^{3+} (0.67 Å) and Ru^{3+}

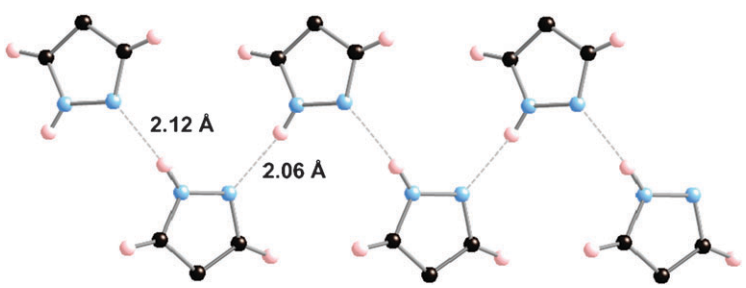

Fig. 8 Zigzag hydrogen bond pattern formed between the two halves of the organic layer in SrL_2.

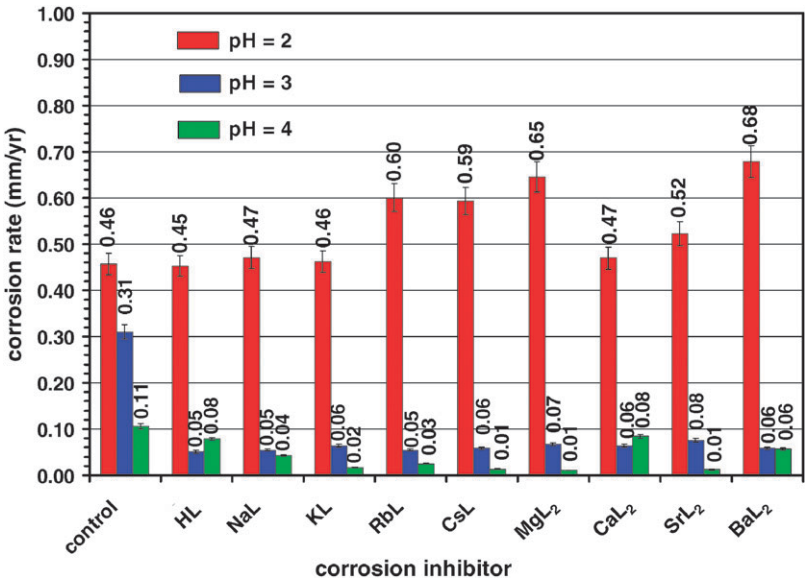

Fig. 10 Copper corrosion rates at pH 2, 3 and 4. Substantial corrosion inhibition is noted by HL and metal–L additives.

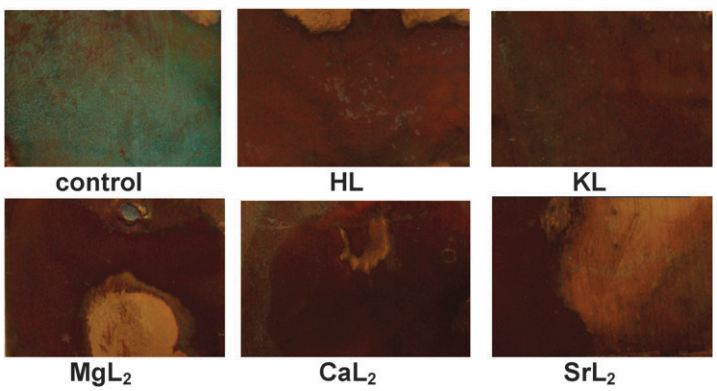

Fig. 11 Selected images of unprotected (control) and protected surfaces at pH 4. Approximate size of each image is 1.0 × 1.5 cm.

(0.68 Å) form hexahydrates $[M(H_2O)_6]^{3+}$ with no sulfonate groups coordinating.[23,24] The larger Cd^{2+} (0.95 Å) and Ca^{2+} (1.00 Å) ions are also 6-coordinate but have one or two η^1-sulfonates coordinating, respectively.[21,25] Similarly sized but higher charged Y^{3+} (1.02 Å) and Ln^{3+} [Ln = Sm (1.08 Å), Eu (1.07 Å), Gd (1.05 Å), Tb (1.04 Å), Dy (1.03 Å), Ho (1.02 Å), Er (1.00 Å), Yb (0.98 Å) and Lu (0.98 Å)] are 8-coordinate, with two η^1-sulfonate groups and six H_2O molecules coordinating.[22,26,27] Interestingly, the even larger lanthanides La^{3+} (1.22 Å), Ce^{3+} (1.20 Å) and Nd^{3+} (1.16 Å) have no sulfonates coordinating and form isostructural complexes containing 9-coordinate $[M(H_2O)_9]^{3+}$ species,[27] similarly to Bi^{3+} (~1.2 Å) in $[Bi(H_2O)_9]^{3+}(F_3CSO_3)_3$.[28] The Na^+, Cs^+ and Ag^+ complexes reported are anhydrous. The Na^+ ion (1.02 Å) is 6-coordinate by five sulfonate groups (four η^1 and one η^2).[29] The Cs^+ ion (1.78 Å) is 9-coordinate by six sulfonate molecules (three η^1 and three η^2).[30] In the case of the Ag^+ complex, infinite zigzagging Ag-chains (Ag–Ag distances of 3.354(1) Å) are interconnected by μ_5-η^2:η^2:η^1 sulfonate groups, with each Ag ion (~1.2 Å, taking into consideration the two short Ag–Ag contacts also) coordinated by five sulfonate groups.[31]

The nature of the backbone of the sulfonate groups also affects the number of coordinated sulfonates and H_2O molecules. For example, from the 22 Mg^{2+} sulfonate structures found in the Cambridge Structural Database (CSD)[32] (with no other functional groups than sulfonate coordinating to Mg), 20 structures based on aromatic sulfonates contain $[Mg(H_2O)_6]^{2+}$ and no sulfonate groups coordinating, while two structures containing the aliphatic hydroxymethyl-[33] and trifluoromethyl-sulfonates[34] have two (η^1) or even six (μ_3-η^1:η^1:η^1) sulfonate groups coordinating, respectively. The non-coordination of the aromatic sulfonates can be attributed to the diminished negative charge on the sulfonate groups due to delocalization over the aromatic ring, which in turn participates in extended π–π interactions. We have found that in $[Mg(H_2O)_6](4\text{-}SO_3\text{-}pzH)_2$, the aromatic pyrazole rings do not form an extended network, but isolated π–π stacks. This can be attributed to the fact that the pyrazole rings are involved in extensive hydrogen bonding, being

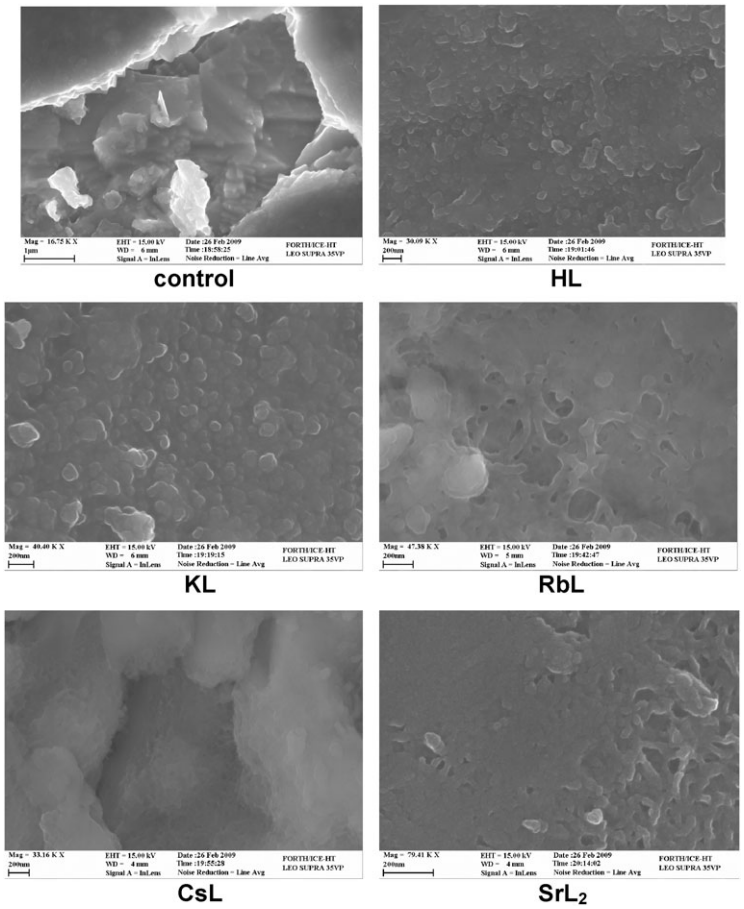

Fig. 12 SEM images of protective metal–L films on copper surfaces. All bars are 200 nm, except the control, 1 μm.

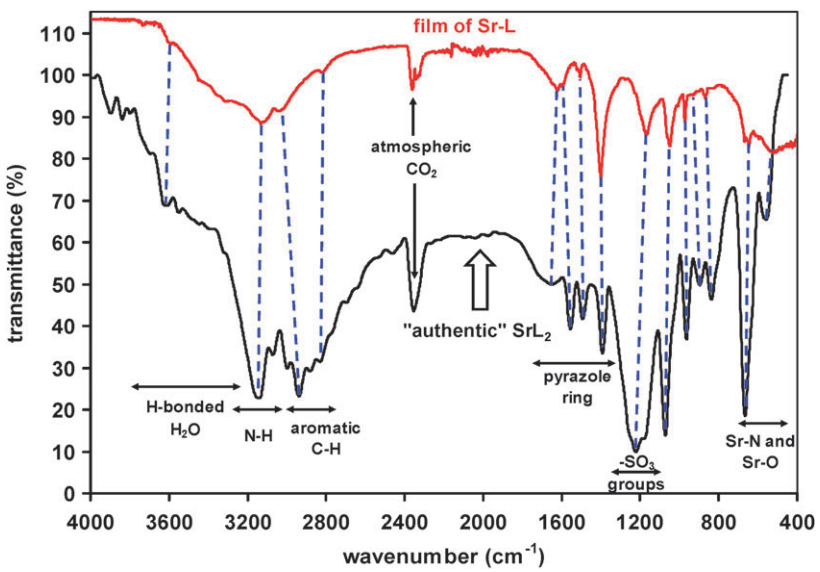

Fig. 13 Comparative FT-IR spectra of the protective SrL_2-film (upper) and an authentic sample of SrL_2.

both H-donors and H-acceptors (unlike the sulfonate backbones of other reported Mg complexes), and that the directional nature of the hydrogen bonds formed disfavors an extended π–π network.

Finally, the number of coordinated sulfonate *vs.* solvent molecules is determined by the polarity of the solvent. While Co^{2+} phenylsulfonate crystallizes as the hexahydrate $[Co(H_2O)_6]^{2+}$ from water,[35] crystallization from anhydrous

Table 8 Ionic radii and structural parameters for metal-pyrazole-4-sulfonate complexes

Cation	Ionic radius[a]/Å	Coordination number	Number of coordinated H_2O molecules	Sulfonate coordination mode	Aromatic interaction pattern	Inorganic layer separation/Å	Ref.
Na^+	1.02	6	4	μ_2-η^1:η^1	Herringbone	10.29	6
K^+	1.51	8	2	μ_4-η^2:η^2:η^2	Sandwich-herring-bone	9.96	6
Rb^+	1.61	8	0	μ_4-η^2:η^2:η^2	Extended T-stacked	6.90	This work
Cs^+	1.78	9	0	μ_5-η^3:η^2:η^2	Sandwich-herring-bone	8.82	This work
Mg^{2+}	0.72	6	6	—	Individual stacks	6.79	This work
Ca^{2+}	1.06	7	3	μ_2-η^1:η^1 and η^1	Brickwall	8.96	6
Sr^{2+}	1.26	8	0	μ_4-η^2:η^1:η^1 and $_3$-η^1:η^1:η^1	Herringbone	14.17	This work
Ba^{2+}	1.52	10	1	μ_4-η^2:η^2:η^1 and $_2$-η^2:η^1	Herringbone strips	8.33	6
Cu^{2+}	0.73	6	2	η^1	Stacked columns	6.65	This work

[a] Effective ionic radii correspond to the observed coordination numbers.[19]

ethanol gives $Co(PhSO_3)_4(EtOH)_2$, with four μ_2-η^1:η^1 sulfonates coordinating to the cobalt ion.[36]

Structure of the organic layer

Variation of the metal ion induces significant changes also in the structure of the organic layer, illustrated by a variety of π–π stacking and edge-to-face aromatic interactions between the pyrazole rings (Fig. 4). The extent of the aromatic interactions is directly proportional to cation size. With the smaller Mg^{2+} and Cu^{2+} ions, individual π–π stacks (0-D) or infinite π-stacked columns (1-D) are observed, respectively. In the case of the larger ions, the pyrazole rings are arranged in infinite 2-D networks having the following patterns: brickwall (Ca^{2+}), herringbone (Na^+ and Sr^{2+}), sandwich-herringbone (K^+ and Cs^+), herringbone strips (Ba^{2+}) and extended T-stacks (Rb^+). Besides aromatic interactions, the pyrazole moieties also participate in hydrogen bonding both as donor and acceptor. These hydrogen bonds formed with sulfonate groups, H_2O molecules or even other pyrazole moieties (in SrL_2) provide additional lattice strength.

The pyrazole groups coordinate through the N-atom to the larger (Rb^+ and Cs^+) or doubly charged (Ca^{2+} and Ba^{2+}) s-metals as well as to the small d-metal Cu^{2+}, but not to Na^+, K^+, Mg^{2+} and Sr^{2+}. An η^1-coordination of the N-atom is observed in the Ca^{2+}, $Ba^{2+}$and Cu^{2+} complexes, while a bifurcated η^2-bridging mode is seen for Rb^+ and Cs^+. Within these structures, while the pyrazole moiety coordinates to one inorganic layer, the sulfonate group of the same 4-SO_3-pzH ligand coordinates to a metal in the next inorganic layer. As a result, the 4-SO_3-pzH ligands act as pillars between two adjacent inorganic layers and lead to shorter interlayer distances (defined here as the distance between the centers of two adjacent inorganic layers) of 6.65(1)–8.96(1) Å as opposed to 9.96(1)–14.17(1) Å in the non-pillared complexes (Na, K, Mg and Sr) (Table 8). An exception is the Mg complex with a short interlayer distance of 6.79(1) Å; in this unique case, the collapse of the organic layer is attributed to the fact that neither the N-atom nor the sulfonate group is coordinating to Mg^{2+}, therefore the pyrazole–sulfonate ligands are not perpendicular to the inorganic layer.

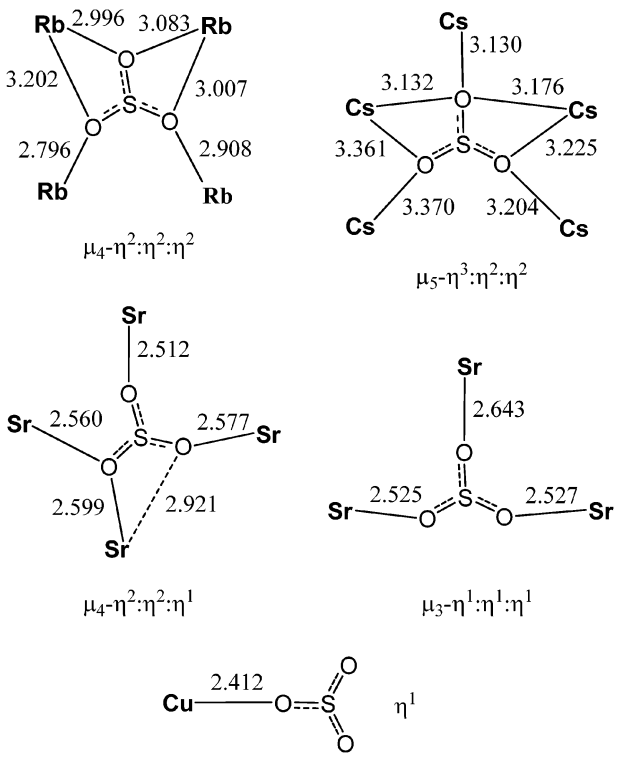

Scheme 2 Coordination modes (hapticity) of the sulfonate group (this work).

Copper corrosion inhibition studies

It is well established that the presence of a heterocyclic N-atom in corrosion inhibitors augments anti-corrosion efficiency.[7] We find indeed that HL inhibits copper corrosion at pH values higher than 2. For example, at pH 4 a corrosion rate of 0.079 mm/year is measured in the presence of HL, which is lower than in the absence of HL (control, 0.106 mm/year). However, this rate is much higher than in the presence of the parent compound, pyrazole alone (0.0021 mm/year). The presence of the sulfonate group in ligand HL increases the water solubility of the latter compared to pyrazole, thus decreasing its filming capability and by consequence, its corrosion protection efficiency. It has been shown that inhibition agents that form soluble species with the corrosion products offer decreased corrosion protection.[8] The product of the copper corrosion experiment in the presence of HL was isolated from the solution and found to be a copper–L complex.

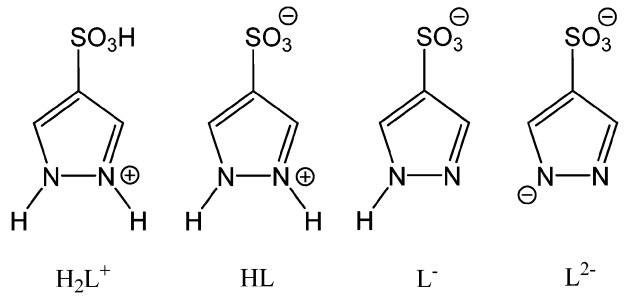

Scheme 3 Possible protonation forms of pyrazole-4-sulfonic acid (HL).

Comparison of corrosion rates in the absence and presence of HL at different pH values reveals that while at pH 2 there is no corrosion inhibition, at pH 3 and 4 there is a large decrease in corrosion rate in the presence of HL. This observation can be explained by the presence of varying amounts of different protonation forms of the ligand HL at different pH values (Scheme 3). In the pH range used in our studies, only HL and L^- have significant contributions; the other two possible species, H_2L^+ and L^{2-} are expected to form only at very low (negative) and very high (distinctly basic) pH values, respectively, and are not invoked in this discussion. While measuring the pK_a value for the HL/L^- system by pH-titration, we found that using HL solutions of different concentrations (0.1–100 mM) provides different pK_a values, suggesting ligand aggregation as concentration increases. We have also observed that while a 0.1 mM solution of HL has a pH of 4.03 which corresponds to 93% of HL being deprotonated, the 1 mM, 10 mM and 100 mM solutions have pH values of 3.08, 2.15 and 1.26, corresponding to 83%, 71% and 55% dissociation, respectively. Single crystal X-ray analysis of HL shows two strong hydrogen bonds for each pair of HL molecules in the solid state.[6] The existence of hydrogen bonded dimers or oligomers (Scheme 4) in increasingly concentrated solutions of HL explains the varying degrees of dissociation (varying pK_a values). Since the corrosion experiments were conducted at 0.5 mM concentrations of HL, we determined the pK_a at this concentration and the obtained value of 3.6 will be used to interpret the results. Based on the Henderson–Hasselbalch equation, at pH 2 only 2% of the ligand is in the form of L^-, while at pH 3 and 4 there is 17% and 67% of L^-, respectively. The corrosion rate at a given pH depends on both [H^+] and concentration of the active corrosion inhibitor species. At pH = 2, the effect of high [H^+] is dominant and the result is a high CR (0.46 mm/yr). At pH = 3, [H^+] is reduced by an order of magnitude and the effects of (reduced) [H^+] and active inhibitor result in a significantly lower CR (0.05 mm/yr). The higher than expected CR value at pH 4 (0.078 mm/yr) is attributed to either the presence of buffer used to raise the pH of the solution to 4 (in the absence of buffer, a 0.5 mM solution of HL has a pH of 3.37) or/and the dramatic increase of [L^-] (67%), compared to the significantly lower [L^-] (17%) at pH = 3. It is well established that increase in anionic inhibitor concentration may have detrimental effects on CR.[17,18]

A similar but even more pronounced trend in corrosion protection efficiency is observed in the presence of metal–L inhibitors. No corrosion protection or even accelerated corrosion is observed at pH 2, significant corrosion protection is achieved at pH 3 and the lowest corrosion rates are observed at pH 4. At pH 2, most corrosion rates are increased compared to the control (Fig. 10). At this pH, the ligand from the metal–L compounds is protonated (98% HL) and the accompanying metal cations aid in the dissolution of the corrosion products. At pH 3, only 83% of the ligand is protonated; the remaining L^- species adsorb unto the copper surface offering protection. The very small variance in corrosion rates in the presence of HL or different metal–L complexes imply a negligible participation of the respective metal cations in corrosion protection (Fig. 10). The further reduced and varying corrosion rates observed at pH 4 (Fig. 10) suggest that the alkali or alkaline-earth cations do participate in corrosion protection; at this pH, 67% of the ligand is in the form of L^-. Indeed, EDS studies confirmed the presence of the respective alkali or alkaline-earth metals in the protective films formed on the copper metal surfaces. The different corrosion rates observed in the presence of different metal–L complexes point to the varying robustness/compactness of the resulting metal–L films. The best corrosion protection (at pH 4) is achieved in the presence of Mg^{2+} (0.012 mm/year), while Ca^{2+} offers the least protection (0.085 mm/year).

Conclusions

Herein we have shown that the pyrazole-4-sulfonate anion (4-SO_3-pzH = L^-) can be used to construct layered materials having a variety of 3-D structures. None of the nine structures studied so far are isomorphous. The versatility of the ligand stems from its capability to coordinate to metals *via* both its sulfonate group and aromatic N-atom, and to participate in the same time in hydrogen bonding both as donor and acceptor and in extended aromatic π–π networks. Variation of cation size and/or charge results in profound structural changes within these frameworks. Increasing size or charge of the metal cation is reflected in higher coordination numbers around those metals, larger hapticity of the sulfonate groups as well as less hydration of the metal centers. There is no direct correlation between the size or charge of the cation and interlayer distance. X-ray crystallography shows that in each of the nine pyrazole-4-sulfonate structures, all oxygen, nitrogen as well as O–H and N–H hydrogen atoms are

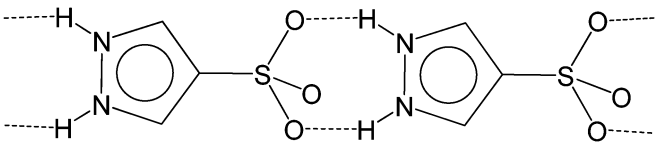

Scheme 4 Hydrogen bonding in pyrazole-4-sulfonic acid (HL).

involved in an extensive hydrogen bond network. We conclude that the overall structure of these complexes is determined by a subtle combination of the coordination preferences of the metal ion and an intricate lattice of hydrogen bonds and aromatic interactions. All alkali and alkaline-earth metal salts of ligand HL show varying copper corrosion protection at pH 3 and 4. The observed corrosion rates are lowest at pH 4 and depend on the nature of different metal–L additives. We are currently studying derivatized pyrazole-4-sulfonate complexes of different metals in order to get further insights into their interesting 3-D supramolecular structures, with an emphasis on improved corrosion protection and other potential applications.

Acknowledgements

We thank Prof. Raphael G. Raptis at the University of Puerto Rico and Prof. Ekkehard Sinn at Western Michigan University for access to the X-ray diffractometers used in this work. G. M. also thanks Western Michigan University for start-up funds.

References

1 (*a*) T. Steiner, *Angew. Chem., Int. Ed.*, 2002, **41**, 48–76; (*b*) G. R. Desiraju, *Acc. Chem. Res.*, 2002, **35**, 565–573; (*c*) L. M. Epstein and E. S. Shubina, *Coord. Chem. Rev.*, 2002, **231**, 165–181; (*d*) G. R. Desiraju and T. Steiner, *The Weak Hydrogen Bond*, Oxford University Press, New York, 1999.

2 (*a*) *Structure and Bonding*, ed. P. Metrangolo and G. Resnati, Springer, Berlin, Heidelberg, New York, 2008, vol. 126; (*b*) P. Metrangolo, F. Meyer, T. Pilati, G. Resnati and G. Terraneo, *Angew. Chem., Int. Ed.*, 2008, **47**, 6114–6127; (*c*) A. Gavezzotti, *Mol. Phys.*, 2008, **106**, 1473–1485; (*d*) K. Rissanen, *CrystEngComm*, 2008, **10**, 1107–1113; (*e*) P. Metrangolo and G. Resnati, *Science*, 2008, **321**, 918–919.

3 (*a*) C. A. Hunter, K. R. Lawson, J. Perkins and C. J. Urch, *J. Chem. Soc., Perkin Trans. 2*, 2001, 651–669; (*b*) C. J. Janiak, *J. Chem. Soc., Dalton Trans.*, 2000, 3885–3896.

4 (*a*) H. Schmidbaur and A. Schier, *Chem. Soc. Rev.*, 2008, **37**, 1931–1951; (*b*) M. J. Katz, K. Sakai and D. B. Leznoff, *Chem. Soc. Rev.*, 2008, **37**, 1884–1895.

5 (*a*) T. Laube, *Chem. Rev.*, 1998, **98**, 1277–1312; (*b*) N. J. Turro, *Chem. Commun.*, 2002, 2279–2292.

6 G. Mezei and R. G. Raptis, *New J. Chem.*, 2003, **27**, 1399–1407.

7 (*a*) M. M. Antonijevic and M. B. Petrovic, *Int. J. Electrochem. Sci.*, 2008, **3**, 1–28; (*b*) P. G. Cao, J. L. Yao, J. W. Zheng, R. A. Gu and Z. Q. Tian, *Langmuir*, 2002, **18**, 100–104; (*c*) Y. S. Tan, M. P. Srinivasan, S. O. Pehkonen and S. Y. M. Chooi, *Corros. Sci.*, 2006, **48**, 840–862; (*d*) S. Ramesh, S. Rajeswari and S. Maruthamuthu, *Appl. Surf. Sci.*, 2004, **229**, 214–225; (*e*) E. Geler and D. S. Azambuja, *Corros. Sci.*, 2000, **42**, 631–643; (*f*) M. A. Elmorsi and A. M. Hassanein, *Corros. Sci.*, 1999, **41**, 2337–2352; (*g*) M. M. Antonijevic, S. M. Milic and M. B. Petrovic, *Corros. Sci.*, 2009, **51**, 1228–1237.

8 K. Babic-Samardzija, C. Lupu, N. Hackerman, A. R. Barron and A. Luttge, *Langmuir*, 2005, **21**, 12187–12196.

9 C. S. Rondestvedt, Jr and P. K. Chang, *J. Am. Chem. Soc.*, 1955, **77**, 6532–6540.

10 (*a*) *Data Collection: SMART-NT Software Reference Manual, version 5.0*, Bruker AXS, Inc., Madison, WI, 1998; (*b*) *Data Reduction: SAINT-NT Software Reference Manual, version 4.0*, Bruker AXS, Inc., Madison, WI, 1996; (*c*) G. M. Sheldrick, *SHELXTL-NT, version 5.1*, Bruker AXS, Inc., Madison, WI, 1999. On the SMART APEX II instrument, the APEX2 v2008.2-0 software package was used.

11 (*a*) NACE Standard TM0169-95 (Item No. 21200), National Association of Corrosion Engineers, Houston TX, USA (www.nace.org); (*b*) K. D. Demadis, C. Mantzaridis, R. G. Raptis and G. Mezei, *Inorg. Chem.*, 2005, **44**, 4469–4471.

12 Rb–N bonds longer than 3.2 Å: (*a*) J. H.N. Buttery, Effendy, S. Mutrofin, N. C. Plackett, B. W. Skelton, N. Somers, C. R. Whitaker and A. H. Z. White, *Z. Anorg. Allg. Chem.*, 2006, **632**, 1839–1850; (*b*) C. Suchentrunk and N. Korber, *Inorg. Chim. Acta*, 2006, **359**, 267–272; (*c*) M. Dobler and R. P. Phizackerley, *Acta Crystallogr., Sect. B: Struct. Crystallogr. Cryst. Chem.*, 1974, **30**, 2746–2748; (*d*) M. Ito, T. Sato, K. Sakai and T. Tsubomura, *Chem. Lett.*, 1996, 619–620.

13 Rb–N–Rb bridging heterocycle: (*a*) A. H. Ilkhechi, J. M. Mercero, I. Silanes, M. Bolte, M. Scheibitz, H.-W. Lerner, J. M. Ugalde and M. Wagner, *J. Am. Chem. Soc.*, 2005, **127**, 10656–10666; (*b*) G. W. Rabe, H. Heise, G. P. A. Yap, L. M. Liable-Sands, I. A. Guzei and A. L. Rheingold, *Inorg. Chem.*, 1998, **37**, 4235–4245; (*c*) H. Esbak and U. Z. Behrens, *Z. Anorg. Allg. Chem.*, 2005, **631**, 1581–1587; (*d*) S. T. Liddle and W. Clegg, *Polyhedron*, 2002, **21**, 2451–2455.

14 Cs–N bonds longer than 3.5 Å: (*a*) J. Ellermann, W. Bauer, M. Schutz, F. W. Heinemann and M. Moll, *Monatsh. Chem.*, 1998, **129**, 547–566; (*b*) S. Dieterich and J. Z. Strahle, *Z. Naturforsch. B*, 1993, **48**, 1574–1580; (*c*) M. Cai, A. L. Marlow, J. C. Fettinger, D. Fabris, T. J. Haverlock, B. A. Moyer and J. T. Davis, *Angew. Chem., Int. Ed.*, 2000, **39**, 1283–1285; (*d*) T. Nabeshima, Y. Yoshihira, T. Saiki, S. Akine and E. Horn, *J. Am. Chem. Soc.*, 2003, **125**, 28–29; (*e*) V. V. Ponomareva, V. V. Skopenko, K. V. Domasevitch, J. Sieler and T. Z. Gelbrich, *Z. Naturforsch. B*, 1997, **52**, 901–905; (*f*) M. Arca, F. Demartin, F. A. Devillanova, A. Garau, F. Isaia, V. Lippolis and G. Verani, *Inorg. Chem.*, 1998, **37**, 4164–4165; (*g*) A. Steiner and D. Stalke, *Inorg. Chem.*, 1993, **32**, 1977–1981.

15 Cs–N–Cs bridging heterocycle: (*a*) C. Suchentrunk and N. Z. Korber, *Z. Naturforsch. B*, 2003, **58**, 990–996; (*b*) I. Heldt, T. Borrmann and U. Z. Behrens, *Z. Anorg. Allg. Chem.*, 2003, **629**, 1980–1985; (*c*) S. T. Liddle and W. Clegg, *J. Chem. Soc., Dalton Trans.*, 2001, 402–408; (*d*) S. T. Liddle and W. Clegg, *Acta Crystallogr., Sect. E: Struct. Rep. Online*, 2003, **59**, m1062–m1064; (*e*) T. Stey, M. Pfeiffer, J. Henn, S. K. Pandey and D. Stalke, *Chem.–Eur. J.*, 2007, **13**, 3636–3642.

16 R. M. Silverstein, G. C. Bassler and T. C. Morrill, *Spectrometric Identification of Organic Compounds*, 4th edn, John Wiley, New York, 1981, pp. 132–133.

17 (*a*) K. D. Demadis, M. Papadaki, R. G. Raptis and H. Zhao, *Chem. Mater.*, 2008, **20**, 4835–4846; (*b*) K. D. Demadis, M. Papadaki, R. G. Raptis and H. J. Zhao, *J. Solid State Chem.*, 2008, **181**, 679–683.

18 (*a*) K. D. Demadis, C. Mantzaridis and P. Lykoudis, *Ind. Eng. Chem. Res.*, 2006, **45**, 7795–7800; (*b*) K. D. Demadis, P. Lykoudis, R. G. Raptis and G. Mezei, *Cryst. Growth Des.*, 2006, **6**, 1064–1067; (*c*) K. D. Demadis, E. Barouda, R. G. Raptis and H. Zhao, *Inorg. Chem.*, 2009, **48**, 819–821; (*d*) K. D. Demadis, E. Barouda, N. Stavgianoudaki and H. Zhao, *Cryst. Growth Des.*, 2009, **9**, 1250–1253.

19 R. D. Shannon, *Acta Crystallogr., Sect. A: Cryst. Phys., Diffr., Theor. Gen. Crystallogr.*, 1976, **32**, 751–767.

20 C. Couldwell, K. Prout, D. Robey, R. Taylor and F. J. C. Rossott, *Acta Crystallogr., Sect. B: Struct. Crystallogr. Cryst. Chem.*, 1978, **34**, 1491–1499.

21 K. R. Fewings, P. C. Junk, D. Georganopoulou, P. D. Prince and J. W. Steed, *Polyhedron*, 2001, **20**, 643–649.

22 Y. Ohki, Y. Suzuki, T. Takeuchi and A. Ouchi, *Bull. Chem. Soc. Jpn.*, 1988, **61**, 393–405.

23 M. A. S. Aquino, W. Clegg, Q.-T. Liu and A. G. Sykes, *Acta Crystallogr., Sect. C: Cryst. Struct. Commun.*, 1995, **51**, 560–562.

24 P. Bernhard, H.-B. Bergi, J. Hauser, H. Lehmann and A. Ludi, *Inorg. Chem.*, 1982, **21**, 3936–3941.

25 (*a*) F. Florencio, S. Martinez-Carrera, S. Garcia-Blanco, M. Bombin, M. A. Martinez-Zaporta, A. Ramirez-Garcia and A. Gerrero-Laverat, *Eur. Cryst. Meeting*, 1985, **9**, 220 (CSD REFCODE: DIMVAW); (*b*) A. Guerrero, A. Ramirez, A. Santos, M. Bombin, M. A. Martinez-Zaporta, F. Florencio, S. M. Carrera and S. G. Blanco, *An. Quim.*, 1990, **86**, 886–891 (CSD REFCODE: DIMVAW01).

26 C. Jones, P. C. Junk, M. K. Smith and R. C. Z. Thomas, *Z. Anorg. Allg. Chem.*, 2000, **626**, 2491–2497.

27 D. L. Faithfull, J. M. Harrowfield, M. I. Ogden, B. W. Skelton, K. Third and A. H. White, *Aust. J. Chem.*, 1992, **45**, 583–594.
28 W. Frank, G. J. Reiss and J. Schneider, *Angew. Chem., Int. Ed. Engl.*, 1995, **34**, 2416–2417.
29 H. Reinke and S. Rudershausen, Private Communication, 1999 (refcode: HORSUC).
30 B. Sun, Y. Zhao, J.-G. Wu, Q.-C. Yang and G.-X. Xu, *J. Mol. Struct.*, 1998, **471**, 63–66.
31 G. K. H. Shimizu, G. D. Enright, C. I. Ratcliffe, G. S. Rego, J. L. Reid and J. A. Ripmeester, *Chem. Mater.*, 1998, **10**, 3282–3283.
32 F. H. Allen, *Acta Crystallogr., Sect. B: Struct. Sci.*, 2002, **58**, 380–388 (ConQuest version 1.10, 2008).
33 T. S. Cameron, W. J. Chute, G. Owen, J. Aherne and A. Linden, *Acta Crystallogr., Sect. C: Cryst. Struct. Commun.*, 1990, **46**, 231–235.
34 R. Dinnebier, N. Sofina, L. Hildebrandt and M. Jansen, *Acta Crystallogr., Sect. B: Struct. Sci.*, 2006, **62**, 467–473.
35 E. J. Kosnic, E. L. McClymont, R. A. Hodder and P. J. Squattrito, *Inorg. Chim. Acta*, 1996, **244**, 253–254.
36 A. Guerrero-Laverat, A. Ramirez, A. Jeronimo, A. Santos, F. Florencio, S. Martinez-Carrera and S. Garcia-Blanco, *Inorg. Chim. Acta*, 1987, **128**, 113–117.